Werk

Jahr: 1977
Kollektion: fid.geo
Signatur: 8 Z NAT 2148:44
Digitalisiert: Niedersächsische Staats- und Universitätsbibliothek Göttingen
Werk Id: PPN1015067948_0044
PURL: http://resolver.sub.uni-goettingen.de/purl?PPN1015067948_0044

LOG Id: LOG_0049
LOG Titel: The theoretical investigation of resistivity methods for geoelectrical prospecting in marine areas
LOG Typ: article

Übergeordnetes Werk

Werk Id: PPN1015067948
PURL: http://resolver.sub.uni-goettingen.de/purl?PPN1015067948
OPAC: http://opac.sub.uni-goettingen.de/DB=1/PPN?PPN=1015067948

Contact

Niedersächsische Staats- und Universitätsbibliothek Göttingen
Georg-August-Universität Göttingen
Platz der Göttinger Sieben 1
37073 Göttingen
Germany
Email: gdz@sub.uni-goettingen.de

J. Geophys. 44, 245–255, 1978

Journal of Geophysics

The Theoretical Investigation of Resistivity Methods for Geoelectrical Prospecting in Marine Areas

J. Sebulke

Technische Universität Berlin, Institut für Angewandte Geophysik, Petrologie und Lagerstättenforschung, Straße des 17. Juni 135, EB 15, 1000 Berlin 12

Abstract. The applicability of the geoelectrical resistivity method in marine areas is studied by model calculations. For a simplified three-layer-model assuming homogeneous and isotropic conditions together with parallel boundaries the apparent resistivity is calculated for three different electrode configurations. It is concluded that for two of the configurations the thickness of layer 2 (sediments) can be determined with a sufficient accuracy.

Key words: Marine geoelectrical sounding – Computed apparent resistivity – Marine Geophysical survey.

1. Introduction

As the demand for mineral raw materials and the geoscientific interest in the oceans have increased, methods primarily used for measurements on land were modified for an application in the marine areas or even totally new techniques were developed. Thus important progresses have been obtained in seismics, gravimetry, geothermics and magnetics which also led to new developments in some subbranches of maringeophysics.

In geoelectrics comparatively few experiments have been published which examine methods for an application at the sea. Sovietic and Dutch authors (Volker and Dijkstra, 1955; Terekhin, 1962; Van' Yan, 1956) have reported about the application of the resistivity methods hitherto used on land.

This article informs about activities to develop special geoelectric resistivity methods suitable for the special conditions at sea. The preferred prospecting object is thin clastic sea floor sediments which, at the present time, cannot be examined neither by seismic nor ultrasonic methods with a sufficient precision.

The experiment shows that one can draw conclusions about the structure of ocean floor sediments at arbitrary water depths from some of the investigated geoelectrical arrays.

2. Potential of a Point Source in a Three – Layer Halfspace at Arbitrary Depths

A very simple model is used for the following observations with different resistivities (Fig. 1). A sediment layer lies on top of an unlimited half-space, here called bedrock, and is covered with water.

The following assumptions have been made to simplify the calculations:

Each layer is homogeneous and isotropic.

The boundaries of the layers are parallel to each other.

The following considerations have been made at the planning of the electrode configurations:

The source point of the potential field shall be near to that part of the ground which is of interest for the measurements. Therefore the current electrodes are placed either in the water layer or in the sediment.

The potential electrodes are always situated in the water layer, preferably on the sea floor.

Three different configurations will be presented for which model calculations have been carried out.

The one-electrode configuration (Fig. 2): The first current electrode is inserted into the sediment, the second one is located at a – from the physical point of view – infinite distance from the array. The two electrodes for the measurement of the potential difference will be separated so that the distance r between E_1 (current electrode) and S_1 (potential electrode) and between S_1 and S_2 always remains the same.

The asymmetrical two-electrode configuration (Fig. 3 a): The current electrodes E_1 and E_2 are inserted either into the sediment or into the water layer (a is the horizontal distance between E_1 and E_2). The electrodes are placed asymmetrically with respect to the centre of the current electrodes as in the preceeding configuration.

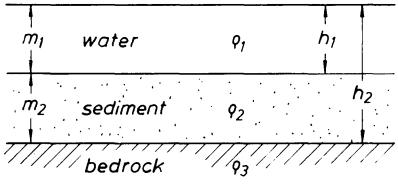

Fig. 1. The model assumed

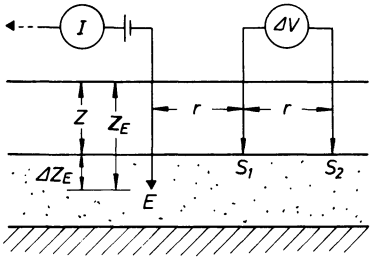

Fig. 2. The one-electrode configuration

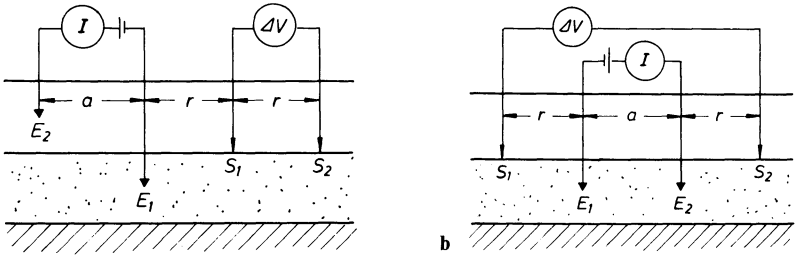

Fig. 3. a The asymmetrical two-electrode configuration. **b** The symmetrical two-electrode configuration

The symmetrical two-electrode configuration (Fig. 3b): The two current electrodes are put at the same depth either into the water layer or on the sea floor, the potential electrodes on the sea floor symmetrically to the current electrodes ($S_1E_1 = S_2E_2 = r$). The potential of arbitrary coordinates of a point source in the half-space has to be known for the calculation of the apparent resistivity $\rho_s(r)$ for each of the described configurations. Each single potential can be calculated by the complementary solution of the Laplace's equation in cylindrical coordinates:

$$V(r,z) = \int_0^\infty [A(\lambda)\, e^{-\lambda z} + B(\lambda)\, e^{\lambda z}]\, J_0(\lambda r)\, d\lambda. \tag{1}$$

The following expressions are obtained for each potential in the different layers n (E_1 and E_2 in layer j):

$$\begin{aligned} V_1 &= V_p + q_j \int_0^\infty (\theta_1(\lambda)\, e^{-\lambda z} + \psi_1(\lambda)\, e^{\lambda z})\, J_0(\lambda r)\, d\lambda \\ V_2 &= V_p + q_j \int_0^\infty (\theta_2(\lambda)\, e^{-\lambda z} + \psi_2(\lambda)\, e^{\lambda z})\, J_0(\lambda r)\, d\lambda \\ V_3 &= V_p + q_j \int_0^\infty (\theta_3(\lambda)\, e^{-\lambda z} + \psi_3(\lambda)\, e^{\lambda z})\, J_0(\lambda r)\, d\lambda \end{aligned} \tag{2}$$

V_p is the primary potential for which the following is valid:

$$V_p = \begin{cases} 0 & \text{for } j \neq n \\ q_j \int_0^\infty e^{-\lambda(z_E - z)} \cdot J_0(\lambda r)\, d\lambda & \text{for } j = n \text{ and } z_E > z \\ q_j \int_0^\infty e^{-\lambda(z - z_E)} \cdot J_0(\lambda r)\, d\lambda & \text{for } j = n \text{ and } z_E < z \end{cases} \tag{3}$$

with:

$$q_j = \frac{\rho_j \cdot I}{4\pi}. \tag{4}$$

The symbols of the parameters are the same as previously used by Flathe (1955). On the condition that the current across the surface of the halfspace is zero we get:

$$\theta_1(\lambda)=\begin{cases}\psi_1(\lambda)+e^{-\lambda z} & \text{for } j=1\\ \psi_1(\lambda) & \text{for } j\neq 1.\end{cases} \tag{5}$$

The condition

$$\psi_3(\lambda)=0 \tag{6}$$

results from the claim that the potential has to disappear at an infinite distance.

The boundary conditions of the stationary electrical field, applied to the generally formulated potentials yield a system of 2 $(n-1)$ equations which determines the same number of initially arbitrary chosen functions $\theta_n(\lambda)$ and $\Psi_n(\lambda)$.

The potentials of an electrode in the different layers j for a point in the layer 1 are as follows:

$j=1$:

$$V(r,z)=q_1\left[\frac{1}{(r^2+(z-z_E)^2)^{1/2}}+\frac{1}{(r^2+(z+z_E)^2)^{1/2}}\right.$$
$$+\int_0^\infty \frac{k_1(e^{-\lambda(2h_1-z_E)}+e^{-\lambda(2h_1+z_E)})+k_2(e^{-\lambda(2h_2-z_E)}+e^{-\lambda(2h_2+z_E)})}{1-k_1e^{-2\lambda h_1}-k_2e^{-2\lambda h_2}+k_1k_2e^{-2\lambda(h_2-h_1)}}$$
$$\left.\cdot(e^{-\lambda z}+e^{\lambda z})J_0(\lambda r)\,d\lambda\right] \tag{7a}$$

$j=2$:

$$V(r,z)=q_2(1-k_1)\int_0^\infty \frac{(e^{-\lambda z_E}+k_2e^{-\lambda(2h_2-z_E)})(e^{-\lambda z}+e^{\lambda z})}{1-k_1e^{-2\lambda h_1}-k_2e^{-2\lambda h_2}+k_1k_2e^{-2\lambda(h_2-h_1)}}J_0(\lambda r)\,d\lambda \tag{7b}$$

$j=3$:

$$V(r,z)=q_3(1-k_1)(1-k_2)$$
$$\cdot\int_0^\infty \frac{e^{-\lambda z_E}(e^{-\lambda z}+e^{\lambda z})}{1-k_1e^{-2\lambda h_1}-k_2e^{-2\lambda h_2}+k_1k_2e^{-2\lambda(h_2-h_1)}}J_0(\lambda r)\,d\lambda \tag{7c}$$

where

$$k_n=\frac{\rho_{n+1}-\rho_n}{\rho_{n+1}+\rho_n}$$

k_n is called the resistivity contrast between neighbouring layers.

These results correspond to those of other authors who examined the potentials of burried current electrodes (Alfano, 1962; Merkel, 1971). All potentials can be written as:

$$V(r,z)=q_j\left(A_j+C_j\int_0^\infty \frac{\sum_i g_i e^{-2\lambda b_i}}{1-k_ie^{-2\lambda h_1}-k_2e^{-2\lambda h_2}+k_1k_2e^{-2\lambda(h_2-h_1)}}J_0(\lambda r)\,d\lambda\right). \tag{8}$$

Substituting $u=e^{-2\lambda h_0}$ and $b_i=m_i\cdot h_0$, where h_0 is the unit length, the integrand of each expression for the potentials (7a–7c) can be transformed into the product of a

rational function and the Bessel function of zero order when only integer multiples of the unit length h_0 are permitted:

$$V(r, z)=q_j\left(A_j+C_j\int_0^\infty \frac{\sum_i g_i u^{m_i}}{P(u)} J_0(\lambda r)\, d\lambda\right) \tag{9}$$

where

$$P(u)=1-k_1 u^\alpha-k_2 u^\beta+k_1 k_2 u^{\beta-\alpha} \tag{10}$$

and

$$\alpha=\frac{h_1}{h_0}\cdot \beta=\frac{h_2}{h_0}. \tag{11}$$

Each rational function can be expressed as power series following the increasing powers of its argument. Consequently the improper integrals can be transformed into infinite convergent series by means of the Weber-Lipschitz formula:

$$\int_0^\infty e^{-b\lambda} J_0(a\lambda)\, d\lambda=\frac{1}{(a^2+b^2)^{1/2}} \quad (b>0). \tag{12}$$

The general expression for the potentials (9) is:

$$V(r, z)=q_j\left(A_j+C_j\sum_{n=1}^\infty \frac{B_n}{(r^2+(2nh_0)^2)^{1/2}}\right) \tag{13}$$

where

$$\frac{\sum_i g_i u^{m_i}}{P(u)}=\sum_{n=1}^\infty B_n u^{n-1}. \tag{14}$$

3. The Apparent Resistivity

The apparent resistivity of the arrays described above is given by

$$\rho_s=K\frac{\Delta V}{I} \tag{15}$$

where K is the configuration factor which depends only on the geometrical part of the array. K has the dimension of m. It is defined in such a way that $\rho_s(r)$ corresponds to the true specific resistivity when Equation (15) has been applied for the homogeneous half-space. To find K, the potential difference ΔV is evaluated for the described array in the homogeneous half-space. Generally the potential of a point source is:

$$V_{pq}=\frac{\rho\cdot I}{4\pi}\cdot\frac{1}{R_{pq}}+\frac{\rho\cdot I\cdot k_0}{4\pi}\frac{1}{R^*_{pq}} \tag{16}$$

where: p = index of the current electrode
q = index of the potential probe
Rpq = distance between the current and the potential electrodes
R^*_{pq} = distance between the current electrode p (reflected with respect to the boundary of the half-space) and the potential probe q
k_0 = resistivity contrast between the conducting and the non-conducting half-space.

Using Equation (15) for a two-electrode configuration we get:

$$K = \frac{4\pi}{(1/R_{11} + 1/R^*_{11} - 1/R_{12} - 1/R^*_{12} - 1/R_{21} - 1/R^*_{21} + 1/R_{22} + 1/R^*_{22})}. \tag{17}$$

ΔV has to be evaluated by the expressions of the potential (13) and put into Equation (15) for the calculation of the model graphs of the apparent resistivity. For example the apparent resistivity for an asymmetrical configuration is (provided that E_1 is placed in layer 2 and E_2 *in layer* 1 ($h_1 < z_{E1} < h_2$; $z_{E2} < h_1$)):

$$\begin{aligned}\rho_s = \rho_2(1-k_1)K^*\left[\sum_{n=1}^{\infty}\frac{B_{2n}}{(1+(2nh_0/r)^2)^{1/2}} - \sum_{n=1}^{\infty}\frac{B_{2n}}{(4+(2nh_0/r)^2)^{1/2}}\right] \\ -\rho_1 K^*\left[A^*_1 + \sum_{n=1}^{\infty}\frac{B_{1n}}{((1+a/r)^2+(2nh_0/r)^2)^{1/2}}\right. \\ \left. - \sum_{n=1}^{\infty}\frac{B_{1n}}{((2+a/r)^2+(2nh_0/r)^2)^{1/2}}\right]\end{aligned} \tag{18}$$

where

$$K^* = K/4\pi r$$

and

$$A^*_1 = \frac{r}{(1/R_{21} + 1/R^*_{21} - 1/R_{22} - 1/R^*_{22})}.$$

Those expressions, calculable by a digital computer, have been derived for each of the considered configurations. The computer was of the type CD 6400. The programming language was FORTRAN IV. A detailed description of the mathematical derivation and the computer programs can be found in Sebulke (1973).

4. Results of the Model Calculations

A large number of model graphs has been computed and apparent resistivity curves have been plotted in one diagramm by changing m_2. Only a limited number of results will be presented here. Figure 4a shows the results for a one-electrode configuration (water depth: 10 m, penetration depth of the electrode into the sediment: 10 m). In this case ρ_2 is double as high as ρ_1. The graph shows that it is possible to determine m_2 of up to 20 m with a good accuracy, especially in the region

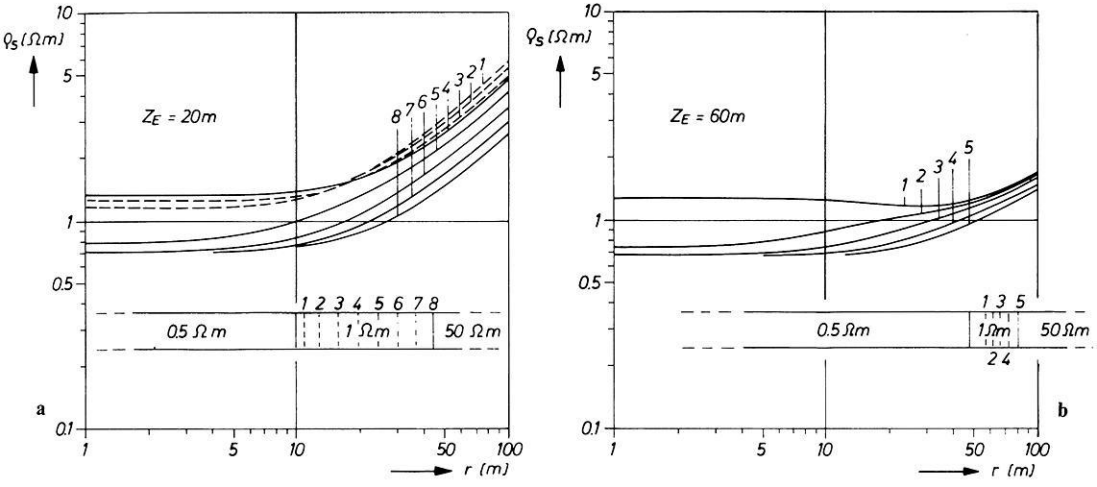

Fig. 4a and b. Computed apparent resistivity for the one-electrode configuration. **a** shallow water; **b** deep water

near the current electrode. The resolving power is made considerably worse with the increase of m_2. It is possible to determine ρ_2 by the curves $\rho_s(r)$ for small r when m_2 is sufficiently large and provided that ρ_1 is known. This value is easely determined. The choice of the ratio ρ_1/ρ_2 is based on practical field measurements in the Mediterranean.

The next Figure 4b shows the results for deeper water buth with the same resistivity ratio. In this case m_1 is 50 m. The source of the electrical field is placed 10 m inside the sediment. The increase in m_1 aggravates only slightly the resolving power. The surface of the water has no influence on the measurements beyond a water depth largely compared with the dimensions of the array. The accuracy of the determination of m_2 is bad when the potential electrodes are on the level of the water surface.

The two-electrode configuration has advantages because the very long supply-line for the second electrode at "infinity" is omitted. A peculiarity of the model graphs for the asymmetrical two-electrode configuration has to be mentioned in this context. K (17) shows a singularity, because the potential difference for this special configuration in the homogeneous half-space disappears for a special distance r. K as a function of the distance r is shown in Figure 5. This behaviour of K determines largely the form of the curves $\rho_s(r)$.

The symmetrical two-electrode configuration (Fig. 3b) gives a slightly improved resolving power for the same ground model (case 1: one-electrode configuration, Fig. 4a). The results are shown in Figure 6. A comparison with results of the one-electrode configuration (Fig. 4a) shows that the gradient of the curves $\rho_s(r)$ with the same parameter differs for large distances r. The resolving power does not change, but as mentioned before, the two-electrode configuration has some advantages with respect to the measuring procedure. A towed multiple conductor cable with electrodes at fixed distances r and an apparatus adapted to

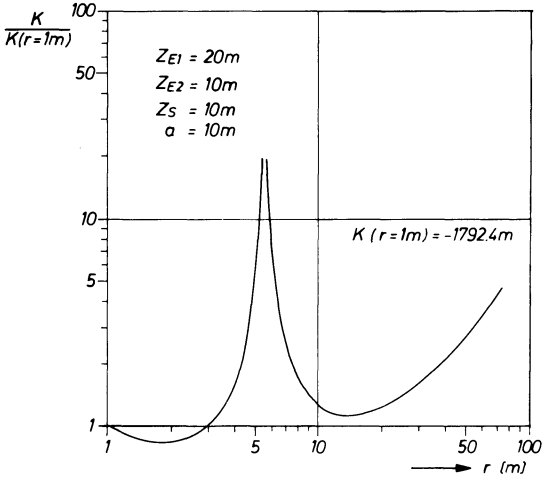

Fig. 5. The configuration factor for the asymmetrical two-electrode configuration

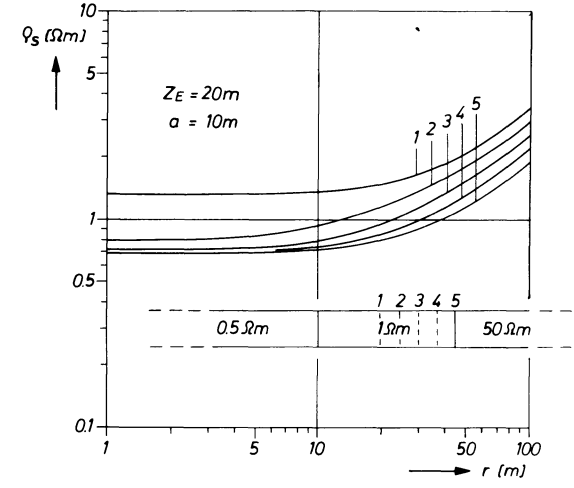

Fig. 6. Computed apparent resistivity for the symmetrical two-electrode configuration

the particular measurement conditions at sea have been constructed. It will be described by Bischoff in a later publication.

The asymmetrical two-electrode configuration has some measuring advantages, e.g. only one electrode cable, and at the same time a high resolving power may be expected.

The same model as before ist considered for the first example of calculation (Fig. 7a). The current electrodes have a horizontal separation of $a = 10$ m. The electrode E_1 (see Fig. 3a) is inserted into the sediment, electrode E_2 is situated in the water layer. The singularity of the curve is caused by K. The model calculation show strong variations between the $\rho_s(r)$-curves for different thicknesses of m_2. Figure 7a shows that in this special case h_2 can be determines up to a thickness $m_2 = 40$ m with an accuracy of ± 1 m. Even a relative reduction of ρ, does not impair the

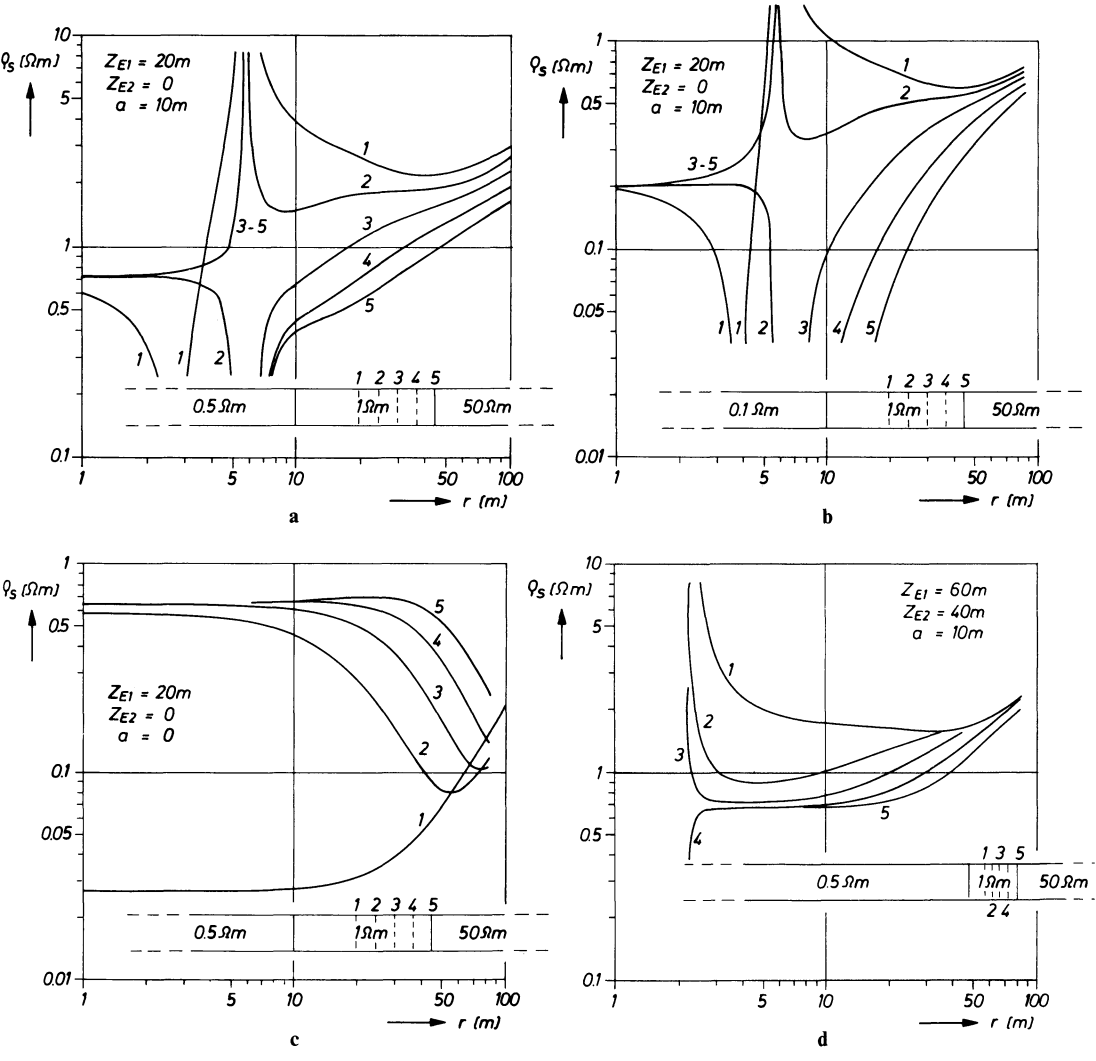

Fig. 7a–d. Computed apparent resistivity for the asymmetrical two-electrode configuration (Electrodes in different layers). **a** shallow water; **b** shallow water, $\rho_1/\rho_2 = 0{,}1$; **c** current electrodes perpendicular one upon another; **d** deep water

interpretation accuracy (Fig. 7b). These model calculations have been made for the same configuration but with a ratio of $\rho_1/\rho_2 = 0{,}1$.

A high efficiency will be obtained when the two sources are perpendicular to each other. The results of this geometrical array are shown in Figure 7c. Again the hitherto most frequent physical model is used. But measuring problems will arise for this version of the asymmetrical configuration because the potential differences between the electrodes at a current of $I = 1\ A$ go down to $\Delta V = 4\ \mu V$ ($m_2 = 15$ m). The calculations for this special array were checked by the aid of model measurements

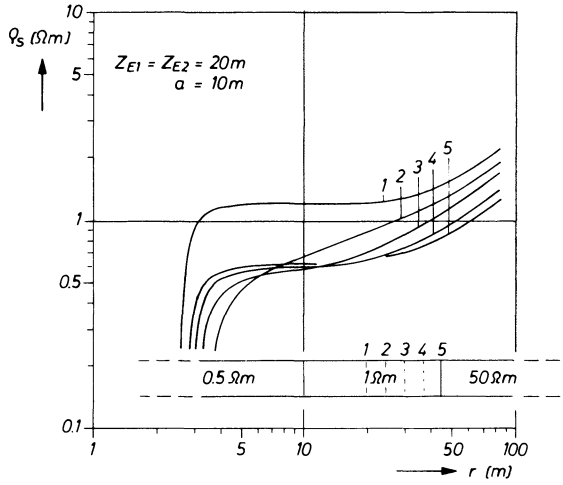

Fig. 8. Computed apparent resistivity for the asymmetrical two-electrode configuration (Both electrodes in the second layer)

in an electrolytical trough (Bischoff, 1973), and a good conformity has been observed.

A removal of the whole array deeper into the water layer aggravates the resolving power in relation to changes of m_2. Figure 7d shows the model graphs for $h_1 = 50\,\text{m}$. But the curves differ well enough to determine m_2 up to 30 m with a sufficient accuracy. The change of the position of electrode E_2 from the water layer into the layer 2 does not improve the interpretation accuracy and even aggravates the resolvin power (Fig. 8).

5. Conclusion

Each of the three configurations examined is suitable for marine geophysical prospecting, but the one-electrode configuration will be excluded because of additional technical expenses. In spite of the small values of ρ_1, the curves $\rho_s(r)$ are sensitive enough to changes of m_2 and ρ_2, so that h_2 can be determined with a sufficient accuracy.

Each method gives useful results even for large water depths. ρ_1 and ρ_2 can be determined by additional measurements and by the behaviour of the sounding curves for small distances r. m_1 can be measured and the problem to determine m_2 is conditionally unique, provided that the prospected object can be described by a three-layer model.

Acknowledgements. I would like to thank Prof. Dr. J. Behrens and Prof. Dr. A. Wilke for some useful discussions and their interest in this problems. Thanks are due to all my colleagues who helped with the measuring in the Mediterranean.

References

Alfano, L.: Geoelectrical prospecting with underground electrodes. Geophys. Prospecting **10**, 290–303, 1962

Bischoff, J.: Eine Apparatur für die Durchführung modellgeoelektrischer Arbeiten nach der Widerstandsmethode zur Simulierung von geoelektrischen Messungen im marinen Bereich. Diplomarbeit, Berlin 1973

Flathe, H.: A practical method of calculation geoelectrical model graphs for horizontal stratified media. Geophys. Prospecting **3**, 268–294, 1955

Merkel, R. H.: Resistivity analysis for plane-layer-half-space models with burried current sources. Geophys. Prospecting **19**, 626–639, 1971

Sebulke, J.: Entwicklung und Untersuchung einer Widerstandsmethodik zur geoelektrischen Prospektion im marinen Bereich. Dissertationschrift D 83, Technische Universität, Berlin 1973

Terekhin, E. I.: Theoretical bases of electrical probing with an apparatur immersed in water. In: Applied Geophysics U.S.S.R. p. 169–195, Oxford: Pergamon Press 1962

Van'Yan, L. L.: Theoretical curves for electrical sea probing with a sea-bottom apparatus. Applied Geophysics Nr. 50, Gostoptekhizdat 1956

Volker, E., Dijkstra, J.: Determination des salinites des eaux dans le sous-sol du Zuiderzee par prospection geophysique. Geophys. Prospecting **3**, 111–125, 1955

Received January 6, 1977/Revised Version October 3, 1977